Analyst

High-performance Hg2+ FET-type sensors based on reduced graphene oxide/polyfuran nanohybrids

Journal:	*Analyst*
Manuscript ID:	AN-COM-02-2014-000403.R1
Article Type:	Communication
Date Submitted by the Author:	31-Mar-2014
Complete List of Authors:	Park, Jin Wook; Seoul National University, Chemical and Biological Engineering Park, Seonjoo; Seoul National University, Chemical and Biological Engineering Kwon, Oh Seok; Yale University, Chemical and Environmental Engineering School of Engineering and Applied Science Lee, Choonghyeon; Seoul National University, Chemical and Biological Engineering Jang, Jyongsik; Seoul National University,

Cite this: DOI: 10.1039/c0xx00000x

www.rsc.org/chemcomm

COMMUNICATION

High-performance Hg^{2+} FET-type sensors based on reduced graphene oxide/polyfuran nanohybrids

Jin Wook Park,[a] Seon Joo Park[a], Oh Seok Kwon[b], Choonghyen Lee[a] and Jyongsik Jang*[a]

Received (in XXX, XXX) Xth XXXXXXXXX 20XX, Accepted Xth XXXXXXXXX 20XX

DOI: 10.1039/b000000x

A new type of field-effect transistor (FET) sensor, based on reduced graphene oxide (rGO)–polyfuran (PF) nanohybrids, was strategically developed. The sensing transducer exhibited a rapid response (< 1 s) and high sensitivity (10 pM) in a liquid-ion-gated FET-type Hg^{2+} sensor. Excellent Hg^{2+} discrimination in heavy metal mixtures was also monitored in real time.

Mercury (Hg) has been used for decades as a chemical additive and energy source in industrial applications.[1] However, very low concentrations of Hg can be extremely toxic, both to human health and to the environment.[2] Hg has been linked to several fatal diseases, including Minamata disease, pulmonary edema, cyanosis, and nephrotic syndrome.[3] Thus, an accurate and sensitive Hg detection method is important to the health care and environmental fields. Several methods have been developed for Hg sensing, including photoelectrochemical methods, colorimetric analysis, and oligonucleotide-based sensing.[4] These methods, however, have significant drawbacks, including slow response, high cost, complicated equipment requirements, and lack of high sensitivity and selectivity. Recently, rapid and reliable Hg sensing performance has been reported for surface-functionalized electrochemical sensors.[5] However, these electrochemical sensors require complicated electrode fabrication, modification, and/or the synthesis of modifiers, such as complexing agents. Thus, the development of simple, high-performance Hg detection systems is desired.

Nanoscale conducting polymers (NCPs) have been used for detection of toxic metal ions via adsorption by their functional groups.[6] NCPs have many advantages, including ease of fabrication, good biocompatibility, and high conductivity.[7] Among these materials, few examples of polyfuran (PF) have been reported. PF showed unique properties compared with other CPs, especially polythiophene (PS) and polypyrrole (PPy), including higher rigidity, better solubility, better packing, and higher fluorescence.[8] Despite these outstanding properties, no study related to the control of PF nanoscale morphology and its functional group exists, owing to the limited availability of PF synthetic method and the poor solubility. In particular, the incomparable functional group of nano-scaled PF is clearly expected effectively to detect the toxic metal ions. Therefore, a systematic study of new NCP-based selective sensing devices toward a specific metal ion (Hg, in this case) is of great interest and significance.

Graphene, which consists of a single layer or a few layers of graphitic carbon, has been extensively investigated for use in many electronics applications due to its large theoretical surface area, good electronic conductivity, mechanical properties, and exceptional thermal stability.[9] Nowadays, graphene composite materials, which show synergetic effects such as enhanced surface area and conductivity, have been reported to selectively detect toxic metal ions in combination with a glassy carbon electrode (GCE).[10] However, this method is limited in practical applications by the requirements for multiple surface functionalization steps and proper oxidation level of the materials. On the other hand, field-effect transistor (FET)-type sensors, which combine sensing and amplification in a single device, have potential for use in miniaturized, portable sensor systems with ultra-sensitive sensing performance.[11] Very recently, aptamer–graphene-based liquid-ion-gated FET sensors with excellent sensing behavior toward toxic metal ions have been reported.[12] However, aptamers typically also exhibit inefficiency, limited stability, and sensitivity to various environmental factors. Thus, the development of a non-aptamer-based sensing device, with high sensitivity and selectivity toward toxic metal ions, is needed.

In this work, for the first time, we report a new class of graphene–PF nanohybrids and their use in liquid-ion-gated FETs for Hg^{2+} detection. Because of high charge carrier mobility along the long axis, PF nanotubes (NTs) in nanohybrids act as molecular probes for detection of Hg^{2+} with high sensitivity and excellent selectivity in FET-type sensors.

Fig. 1 contains a schematic diagram of the synthesis of graphene–PF NT hybrids. First, PF NTs were successfully synthesized via self-degradation.[13] PF NTs were then coupled to

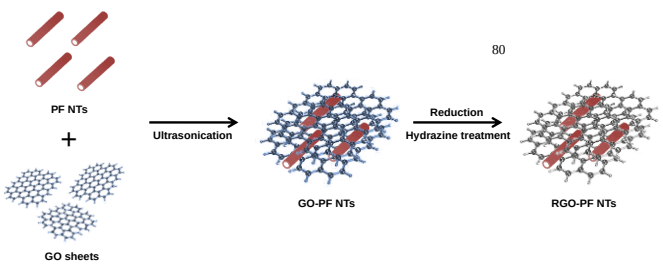

Fig.1 The synthesis of rGO-PF NT hybrids.

the graphene oxide (GO) surface via π–π intermolecular interactions. Hydrazine reduction was then carried out, and the prepared reduced graphene oxide (rGO)–PF NTs were washed several times with distilled water. Finally, the product was obtained by centrifugal precipitation and dried in a vacuum oven at 25℃.

The morphology of the rGO–PF NT hybrids was characterized using scanning electron microscopy (SEM) and transmission electron microscopy (TEM). Fig. 2a shows the SEM and TEM images of the PF NTs, which indicate that the diameter of the tubes was about 70 nm. Fig. 2b shows a cross-sectional SEM image of the rGO sheet, which had a structure resembling paper with porous spaces. Fig. 2c and d show cross-sectional SEM and TEM images of the rGO–PF NT hybrid materials. The structure of the PF NTs was well organized on the large surface area of the graphene sheets. The PF NTs were highly coupled and compacted with the rGO sheets. These results suggested that the rGO–PF NT composites were stable, and the stability was attributed to the strong π–π interactions between the rGO layers and PF NTs.

The electrical properties of the rGO, PF NTs, and rGO–PF NT hybrid materials on the patterned electrode substrate were characterized by measuring current–voltage (I–V) curves. As shown in Fig. 3a, linear I–V curves were observed over a range of –0.6 V to +0.6 V, indicating that Ohmic contacts were formed between samples and the gold electrodes. The conductivity of the rGO–PF NT hybrid was higher than that of rGO and PF NTs. This result suggested that rGO–PF NT composites exhibited effective electron transport between the PF NTs and the rGO, resulting in a decrease in the resistance. Although the rGO sheet exhibited excellent electrical properties, the conductivity was highly anisotropic, and interlayer electron transport was slow. However, the PF NTs acted as conductive channels to connect the rGO layers, resulting in improved conductivity. To investigate the electrical characteristics of the rGO–PF NT conductive channels, we measured the source–drain current–voltage (I_{SD}–V_{SD}) characteristics of liquid-ion-gated transistors under various gate

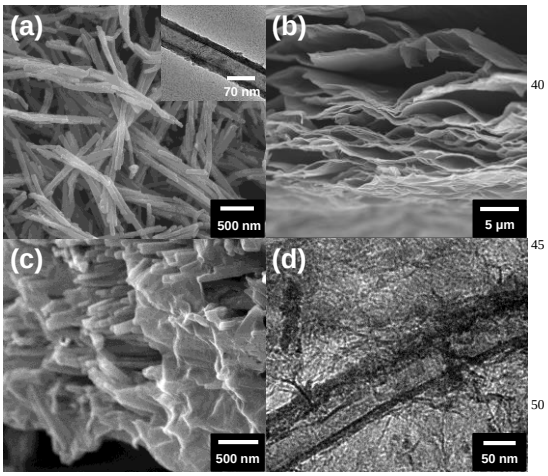

Fig. 2 (a) SEM image of PF NTs; the inset is a TEM image. Cross-sectional SEM images of (b) rGO layers and (c) rGO-PF NTs. (d) TEM image of rGO/PF NTs.

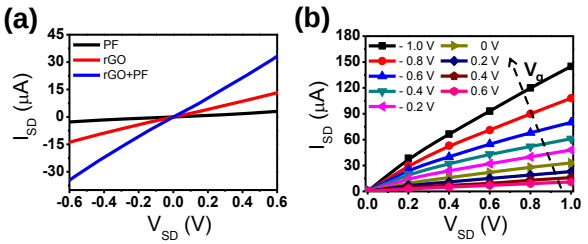

Fig. 3 (a) Current−voltage (I−V) curves of PF NTs, rGO, and rGO-PF NT hybrids and (b) rGO-PF NT composites at V_g from –1.0 to +0.6 V in 0.2-V steps (Vsd: 0 to 1.0 V in 0.2-V steps).

biases. For these measurements, V_g was varied from –1.0 V to +0.6 V in steps of 0.2 V, with a gate voltage sweep rate of 0.2 Vs^{-1}; the devices were in a phosphate-buffered saline (PBS) solution (pH 7.4), as shown in Fig. 3b. I_{SD} increased when a larger negative gate bias was applied, which is typical of *p*-channel transistors. Thus, we concluded that the current in the device was attributable to hole transport and that the modulation of I_{SD} resulted from control over the hole carrier density at the surface of the rGO–PF NT composites. PF NTs exhibited *p*-type semiconductor behavior (see Fig. S2). Although unaltered graphene exhibits ambipolar properties in electrical devices, the graphene samples used herein exhibited hole-transporting behavior due to the absorption of oxygen and/or water from air[14] to yield rGO–PF NT composites that behaved as enhanced *p*-type systems. This behavior, in turn, results in higher stability and improved sensing performance relative to that of the individual components alone.

Liquid-ion-gated FETs were fabricated and immersed in PBS electrolyte at pH 7.4, as shown in Fig. 4a. A remote electrode in the surrounding electrolyte provided good contact between the rGO–PF NT composites and the solution. This strategy enhanced the sensitivity via signal amplification. Using the FET-type sensor as a *p*-channel FET (with V_g = – 0.1 V), the real-time response to Hg^{2+} at various concentrations was observed. The lone-pair electrons on the oxygen atom of furan bind to the Hg^{2+}. As shown in Fig. 4b, the changes in I_{SD} were measured in response to variations in the Hg^{2+} concentration in the solution. The sensitivity was determined from the normalized change in the current $\Delta I_{SD}/I_0 = (I_{SD}–I_0)/I_0$, where I_0 is the initial current and I_{SD} is the measured real-time current following stabilization after adding the Hg^{2+} ion. The I_{SD} of the sensor increased in response to a gradual increase in the concentration of Hg^{2+}, which occurred due to the accumulation of *p*-type charge carriers at the surface of the rGO–PF NT hybrids. Moreover, the real-time responses of the FET-type Hg sensor were rapid (on a time scale of less than 1 s), and instantaneous signal changes were observed over a wide range of Hg^{2+} ion concentrations (10 pM to 100 nM).

The rGO–PF NT composites exhibited very sensitive responses to Hg, with a detection limit of approximately 10 pM [signal-to-noise (S/N) ratio = 3.12]. Typically, S/N ratios of ≥ 3.0 are considered sufficiently high to indicate a significant signal.[15] As shown in Fig. S3, the S/N ratio at the 1 pM level was only 0.89 and thus too low to obtain a reliable signal measurement.

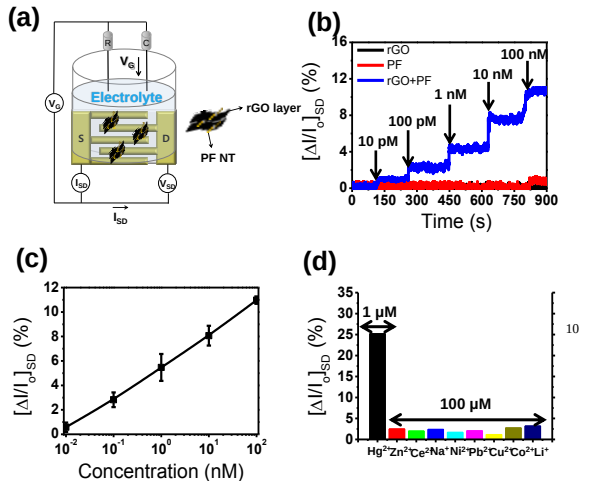

Fig. 4 (a) A liquid-ion-gated FET-type sensor based on rGO-PF NTs. (Ag/AgCl reference electrode, R; platinum counter electrode, C; source and drain electrodes, S and D) (b) Real-time responses and (c) a calibration curve for Hg^{2+} based on rGO, PF NTs; rGO-PF NT composites were measured at Vsd = 10 mV (V_g = – 0.1 V) with Hg^{2+} concentrations of 10 pM to 100 nM. (d) A histogram of the sensitivity of the rGO-PF NT composites to Hg^{2+}, Zn^{2+}, Ce^{2+}, Na^{+}, Ni^{2+}, Pb^{2+}, Cu^{2+}, Co^{2+}, Li^{+}.

Thus, 10 pM is determined to be the detection limit in this system. On the other hand, the FET-type sensor based on PF NTs exhibited a detection limit of about 100 nM (S/N = 3.28). No change in the current after adding the Hg^{2+} was observed for the sensing device based on rGO material alone, thereby indicating that the PF functional groups are critical to sensing performance. Enhanced performance in the sensor based on the rGO–PF NT composites was attributed to the following: (i) an efficient response to Hg^{2+} occurred due to the enhanced surface area and conductivity on the rGO–PF NT hybrid materials, and (ii) the enhanced *p*-type semiconductor behavior improved signal transduction. Figure 4c shows the calibration curve; stronger signals were detected when the Hg^{2+} concentration increased. In all measurements, the FET sensors had rapid response times of less than 1 s and exhibited linear responses to current changes.

The selectivity of the rGO–PF NTs toward Hg^{2+} was evaluated using real-time monitoring of I_{SD} in the presence of various interfering metal ions (e. g., Zn^{2+}, Ce^{2+}, Na^{+}, Ni^{2+}, Pb^{2+}, Cu^{2+}, Co^{2+}, and Li^{+}), as shown in Fig. S4. A remarkable increase in the current was observed when Hg^{2+} ions were injected, even at far lower concentrations (two orders of magnitude) than the other compounds in the analyte (see Fig. 4d). Exposure to other metal ions did not significantly alter the charge density on the surface of the rGO–PF NTs relative to the changes observed upon exposure to Hg^{2+}, because rGO–PF NTs have a greater binding affinity for Hg^{2+} than for the other metal ions.[15,16]

In summary, we demonstrated that rGO–PF NTs can be used for highly sensitive and selective Hg^{2+} detection. The synthesized rGO–PF NT hybrids bound specifically to Hg^{2+} ions. Excellent sensitivity (LOD: 10 pM), selectivity, and a rapid response time of < 1 s were demonstrated in real-time experiments. These FET-type sensors based on rGO–PF NTs have potential for use in new applications and methods for the detection of Hg.

This research was supported by the National Research Foundation of Korea (NRF) grant funded by the Korean government (MEST) (Grant No. 2011-0017125).

Notes and references

[a] *World Class University (WCU) program of Chemical Convergence for Energy & Environment (C2E2), School of Chemical and Biological Engineering, College of Engineering, Seoul National University (SNU), Seoul, Korea. Fax: 82 2 888 1604; Tel: 82 2 880 7069; E-mail: jsjang@plaza.snu.ac.kr*
[b] *Department of Chemical and Environmental Engineering School of Engineering and Applied Science Yale University, New Haven, USA.*
† Electronic Supplementary Information (ESI) available: Details of synthesis and characterization of the rGO-PF NTs as well as the Hg sensing experiment. See DOI: 10.1039/b000000x/

1. J. A. Fernández, J. R. Aboal and A. Carballeira, *Sci. Total Environ.* 2000, 256, 151.
2. (a) J. K. Nicholson, M. D. Kendall and D. Osborn, *Nature*, 1983, 304, 633; (b) G.-B. Jiang, J.-B. Shi and X.-B. Feng, *Environ. Sci. Technol.* 2006, 40, 3672; (c) C. Deng, D. Zhangb, X. Pan, F. Chang and S. Wang, *J. Photochem. Photobiol. B Biol.* 2013, 127, 1.
3. (a) T. W. Clarkson, L. Magos and G. J. Myers, *New Engl. J. Med.* 2003, 349, 1731; (b) S. Ekino, M. Susa, T. Ninomiya, K. Imamura and T. Kitamura, *J. Neurol. Sci.* 2007, 262, 131; (c) D. A. Geier and M. R. Geier, *J. Toxicol. Environ. Health, Part A*, 2007, 70, 837; (d) M. Korbas, S. R. Blechinger, P. H. Krone, I. J. Pickering and G. N. George, *Proc. Natl. Acad. Sci.* 2008, 105, 12108.
4. (a) M. Hollenstein, C. Hipolito, C. Lam, D. Dietrich and D. M. Perrin, *Angew. Chem. Int. Ed.* 2008, **47**, 4346; (b) A. Ono and H. Togashi, *Angew. Chem. Int. Ed.* 2004, **43**, 4300; (c) H. G. Sudibya, Q. He, H. Zhang and P. Chen, *ACS Nano*, 2011, **5**, 1990; (d) N. Dave, M. Y. Chan, P.-J. J. Huang, B. D. Smith and J. Liu, *J. Am. Chem. Soc.* 2010, **132**, 12668; (e) S. V. Wegner, A. Okesli, P. Chen and C. He, *J. Am. Chem. Soc.* 2007, **129**, 3474; (f) L. Zhang, T. Li, B. Li, J. Li and E. Wang, *Chem. Commun.* 2010, **46**, 1476.
5. (a) T. Qian, S. Wu and J. Shen, *Chem. Commun.* 2013, **49**, 4610; (b) T. Qian, C. Yu, S. Wu and J. Shen, *J. Mater. Chem. A*, 2013, **1**, 6539; (c) Z.-Q. Zhao, X. Chen, Q. Yang, J.-H. Liu and X.-J. Huang, *Chem. Commun.* 2012, **48**, 2180.
6. (a) M. Choi and J. Jang, *J. Colloid Interf. Sci.* 2008, **325**, 287; (b) J. Li and X. Lin, *Sens. Actuat. B Chem.* 2007, **124**, 486; (c) J. Li and X.-Q. Lin, *Anal. Chim. Acta*, 2007, **596**, 222; (d) Ş. Ulubay and Z. Dursun, *Talanta*, 2010, **80**, 1461.
7. (a) C. Li, H. Bai and G. Shi, *Chem. Soc. Rev.* 2009, **38**, 2397; (b) S. Logothetidis, *Mater. Sci. Eng. B*, 2008, **152**, 96; (c) H. Yoon, J.-Y. Hong and J. Jang, *Small*, 2007, **3**, 1774.
8. (a) C. C. Ferron, M. C. R. Delgado, O. Gidron, S. Sharma, D. Sheberla, Y. Sheynin, M. Bendikov, J. T. L. Navarrete and V. Hernandez, *Chem. Commun.* 2012, **48**, 6732; (b) O. Gidron, Y. Diskin-Posner and M. Bendikov, *J. Am. Chem. Soc.* 2010, **132**, 2148; (c) J. Ma, S. Li and Y. Jiang, *Macromolecules*, 2001, **35**,

1109; (d) O. Gidron, A. Dadvand, E. Wei-Hsin Sun, I. Chung, L. J. W. Shimon, M. Bendikov and D. F. Perepichka, *J. Mater. Chem. C*, 2013, **1**, 4358.

9. (a) A. K. Geim and K. S. Novoselov, *Nature Mater*. 2007, **6**, 183; (b) A. K. Geim, *Science*, 2009, **324**, 1530.

10. (a) Z.-Q. Zhao, X. Chen, Q. Yang, J.-H. Liu and X.-J. Huang, *Chem. Commun.* 2012, **48**, 2180; (b) C. Yu, Y. Guo, H. Liu, N. Yan, Z. Xu, G. Yu, Y. Fang and Y. Liu, *Chem. Commun.*, 2013, **49**, 6492.

11. (a) J. D. Fowler, M. J. Allen, V. C. Tung, Y. Yang, R. B. Kaner and B. H. Weiller, *ACS Nano*, 2009, **3**, 301; (b) N. Mohanty and V. Berry, *Nano Lett.* 2008, **8**, 4469; (c) H. S. Song, O. S. Kwon, S. H. Lee, S. J. Park, U.-K. Kim, J. Jang and T. H. Park, *Nano Lett.* 2012, **13**, 172.

12. J. H. An, S. J. Park, O. S. Kwon, J. Bae and J. Jang, *ACS Nano*, 2013, **7**, 10563.

13. X. Yang, Z. Zhu, T. Dai and Y. Lu, *Macromol. Rapid Commun.* 2005, **26**, 1736.

14. (a) Z. Sun, Z. Yan, J. Yao, E. Beitler, Y. Zhu and J. M. Tour, *Nature*, 2010, **468**, 549; (b) K.-Y. Shin, J.-Y. Hong and J. Jang, *Adv. Mater.* 2011, **23**, 2113.

15. (a) O. S. Kwon, S. J. Park and J. Jang, *Biomaterials*, 2010, **31**, 4740; (b) J. W. Park, S. J. Park, O. S. Kwon, C. Lee and J. Jang, *Anal. Chem.* 2014, **86**, 1822.

16. (a) M. Sadhukhan and S. Barman, *J. Mater. Chem. A*, 2013, **1**,2752; (b) R. K. Upadhyay, N. Soin and S. S. Roy, *RSC Advances*, 2014, **4**, 3823; (c) R.-X. Xu, X.-Y. Yu, C. Gao, J.-H. Liu, R. G. Compton and X.-J. Huang, *Analyst*, 2013, **138**, 1812.